The Astrophysical Journal, 922:199 (9pp), 2021 December 1 https://doi.org/10.3847/1538-4357/ac323e

Asteroseismology of a High-amplitude δ Scuti Star GSC 4552-1498: Mode Identification and Model Fitting

Xiao-Ya Sun[1], Zhao-Yu Zuo[1], Tao-Zhi Yang[1], Xing-Hao Chen[2], and Hong-Rong Li[1]
[1] Ministry of Education Key Laboratory for Nonequilibrium Synthesis and Modulation of Condensed Matter, School of Physics, Xi'an Jiaotong University, Xi'an 710049, People's Republic of China; zuozyu@xjtu.edu.cn
[2] Key Laboratory for the Structure and Evolution of Celestial Objects, Yunnan Observatories, Chinese Academy of Sciences, Kunming 650216, People's Republic of China
Received 2021 September 20; revised 2021 October 18; accepted 2021 October 19; published 2021 November 30

Abstract

In this paper, the pulsation behavior of high-amplitude δ Scuti star GSC 4552-1498 was analyzed. Using the high-precision photometric data from the Transiting Exoplanet Survey Satellite, two new independent frequencies $F1 = 22.6424(1)\ \mathrm{day}^{-1}$ and $F2 = 28.6803(5)\ \mathrm{day}^{-1}$ were identified for this source, along with the fundamental one $F = 17.9176(7)\ \mathrm{day}^{-1}$, which was previously known. In addition, the classical $O - C$ analysis was conducted to give a new ephemeris formula of $\mathrm{BJD}_{\max} = T_0 + P \times E = 2453321.534716(4) + 0.055811(0) \times E$. The $O - C$ diagram reveals a continuous period increase, but the rate of $(1/P)(dP/dt) = 1.11(3) \times 10^{-7}\ \mathrm{yr}^{-1}$ seems much larger (about hundreds) than predicted by evolution theories, which is long been noticed but not well understood, possibly related to nonlinear mode interaction. Based on frequency parameters (i.e., F, $F1$, and $F2$), a series of theoretical models were conducted by employing the stellar evolution code. It turns out that $F1$ should be a non-radial mode and $F2$ is the second overtone radial mode. Due to the mass–metallicity degeneracy, the stellar parameter of the star can however not be determined conclusively. We suggest high-resolution spectral observation is highly desired in the future to further constrain models. We note GSC 4552-1498 is located on the main sequence in the H-R diagram.

Unified Astronomy Thesaurus concepts: Stellar oscillations (1617); Delta Scuti variable stars (370)

Supporting material: machine-readable tables

1. Introduction

One of the long-standing goals in astronomy is to improve our understanding of stellar evolution by constraining the unknown interior physics of stars. At present, the only method to detect the interior physics of star is astroseismology, which uses the resonant pulsation frequencies of a star to constrain its interior properties from a quantitative comparison to stellar models including different input physics (Aerts 2021). The high-precision time series photometric data from space-based telescopes such as Kepler (Borucki et al. 2010; Balona & Dziembowski 2011; Uytterhoeven et al. 2011) and Transiting Exoplanet Survey Satellite (TESS; Ricker et al. 2015; Antoci et al. 2019) provide us an excellent opportunity to detect the period and amplitude of more pulsation modes besides the fundamental one (Antoci et al. 2019). δ Scuti stars are multi-periodic pulsators with periods in range of 0.02–0.25 days and spectral types from A–F, and locate in the classical Cepheid instability strip across the main sequence (MS) in the H-R diagram. They pulsate in radial as well as non-radial modes (Breger 2000; Qian et al. 2018) excited mainly in the κ mechanism (Breger 2000; Aerts et al. 2010; Antoci et al. 2014; Murphy et al. 2020), usually identified as low-radial-order (n) low-angular-degree (l) pressure (p) modes (Uytterhoeven et al. 2011; Holdsworth et al. 2014). Their masses are generally between 1.5 and 2.5 $M_{\odot}$, which place them in the transition region, that is to say, the lower mass stars with thick outer convective envelope and the massive stars with thin convective shell (Bowman 2017). Thus, these characteristics make them excellent targets for astroseismology, in particular for the detailed studies on the structure and evolution of stars in this transition region (Bowman & Kurtz 2018).

High-amplitude δ Scuti (HADS) stars are a subclass of δ Scuti stars with peak-to-peak light amplitudes larger than 0.3 mag. They are traditionally found to be slow rotators with $\nu \sin i < 30\ \mathrm{km\ s}^{-1}$ and pulsation periods between 1 and 6 hr (McNamara 2000). From the ground-based observations, HADS stars typically have only one or two radial pulsation modes, in the fundamental and/or first overtone mode (Balona et al. 2012; Yang et al. 2018a, 2018b). In recent decades, thanks to the high photometric precision observations from space telescopes, especially in the Kepler mission (Borucki et al. 2010), low-amplitude frequencies can also be found in the frequency spectrum of HADS. For instance, in HADS KIC 5950759, a pair of low-amplitude triplet structures centered on the main frequency was reported by Yang et al. (2018b), which was suggested to be caused by the amplitude modulation of stellar rotation. Furthermore, Bowman et al. (2021) re-analyzed the light variation of this star KIC 5950759 and 12 additional independent frequencies were extracted and regarded as non-radial modes. Another HADS star KIC10284901 also shows a weak amplitude modulation with two frequencies, which might be related to the Blazhko effect (Yang & Esamdin 2019). Moreover, low-amplitude frequencies can also be radial mode and thus lead to the discovery of multimode HADS. By using the Kepler data, three independent frequencies were identified in KIC 10975348, and identified as radial modes, which reclassified this star as a triple-mode HADS (Yang et al. 2021).

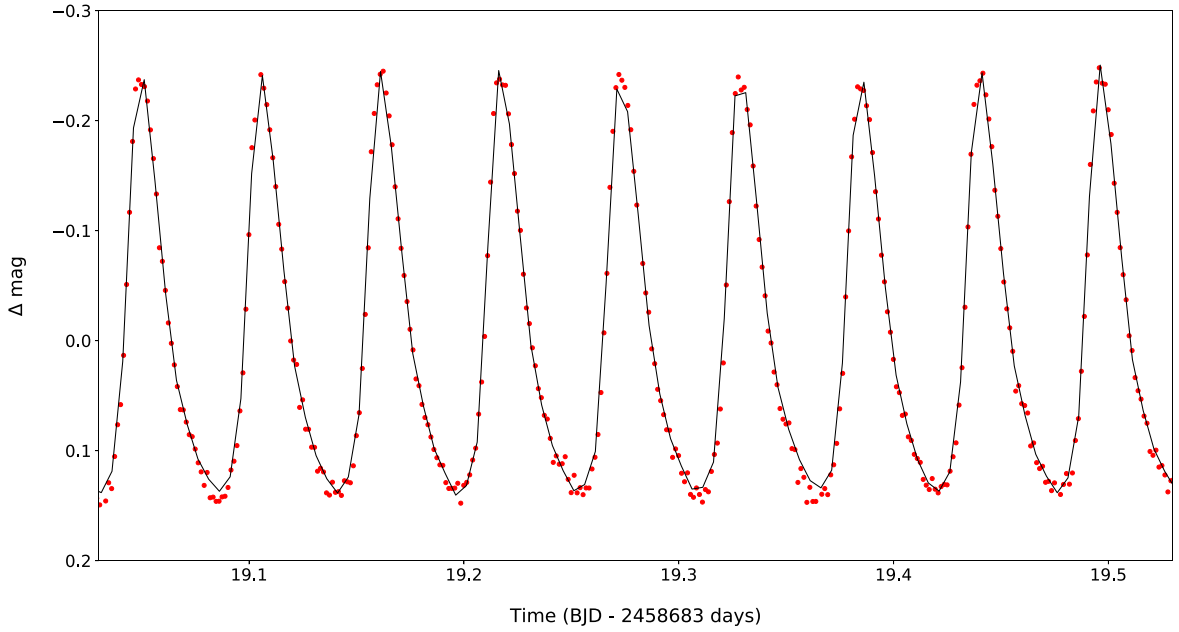

Figure 1. A 0.5 day section of the TESS light curve of GSC 4552-1498. The solid curves represent the fitting with the 13 frequency solutions listed in Table 2. BJD, barycentric Julian date.

Therefore, detection of low-amplitude frequencies will enrich the features of light variation of HADS, and hence provide more information about the internal structure of a star. Based on the high-precision time series photometric data from TESS (Ricker et al. 2014, 2015), more HADS with low-amplitude frequencies pulsation modes (radial and/or non-radial modes) are expected to be detected.

GSC 4552-1498 ($\alpha_{2000} = 11^{h}24^{m}25\overset{s}{.}350$, $\delta_{2000} = +77°42'15\overset{''}{.}629$, 2MASS: J11242535+7742156), was discovered by A.V. Khruslovas, who classified the star as an HADS with a pulsation period of 0.05581096 days. Its amplitude changed from 12.9–13.4 mag (Jafarzadeh & Poro 2017). Jafarzadeh & Poro (2017) derived the frequencies of the fundamental mode $F = 17.899\,\mathrm{day}^{-1}$ and its harmonic $2F = 35.204\,\mathrm{day}^{-1}$ from the ground-based observations. According to the empirical relations, they calculated several parameters of GSC 4552-1498: the effective temperature is $T_{\mathrm{eff}} = 7766 \pm 59$ K, luminosity $L = 9.09 \pm 2.50\ L_{\odot}$, mass $M = 1.68 \pm 0.10\ M_{\odot}$, and the radius is 1.67 $R_{\odot}$. They also obtained four times the maximum light in 2017. During 2009 and 2014, 75 more maxima were collected by Wils et al. (2009, 2012, 2013, 2014, 2015). Some basic parameters of GSC 4552-1498 are listed in Table 1. In order to limit the parameters more accurately and investigate its long-term periodic variation, we downloaded the high-precision photometric data provided by TESS and conducted a detailed study.

2. Observations and Data Reduction

GSC 4552-1498 was observed by TESS (Ricker et al. 2015) during Sectors 14, 20, and 21, from BJD 2458683.346–2458897.782 in 2 min cadence. All the data were downloaded from TESS Asteroseismic Science Operations Center (TASOC) database.[3] In this work, we converted the corrected flux to stellar magnitudes and performed corrections, including eliminating the outliers and detrending the light curve. Then the mean value of each sector was subtracted, and the rectified time series was obtained with 53,568 data points in total, spanning over about 214 days. The typical error per observation of this star is 0.007 mag. A section of the rectified light curves of GSC 4552-1498 is shown in Figure 1. To help the reader visualize the shape of the light curve, a phased curve of GSC 4552-1498 is presented in Figure 2, as well. The light curve shows a faster rise than the decline with a peak-to-peak amplitude of about 0.4 mag, which is typical for HADS stars (McNamara 2000).

3. Frequency Analysis

In this work, the TESS data of GSC 4552-1498 were searched for significant frequencies using PERIOD04 (Lenz & Breger 2005), which was based on the Fourier transformations. The light curve was fitted with the following formula:

$$m = m_0 + \Sigma A_i \sin(2\pi(f_i t + \phi_i)), \quad (1)$$

where m_0 is the zero-point, A_i is the amplitude, f_i is the frequency, and ϕ_i is the corresponding phase.

To detect more significant frequencies, we chose a frequency range of $0 < \nu < 100\,\mathrm{day}^{-1}$, which covers the pulsation frequency of δ Scuti stars, and it is still below the Nyquist frequency ($f_{\mathrm{Ny}} = 1/(2\Delta t) = 360\,\mathrm{day}^{-1}$, i.e., Equation (9) in Murphy et al. (2013), where Δt is the sampling interval between consecutive points). At each step in the process of extracting frequency, the frequency of the highest amplitude peak was determined as a significant frequency, then optimized to the light curve using formula (1), and the solutions of frequency and amplitude were obtained. Then the light curve constructed using the above solutions was subtracted from the data, and the residual was used as input in the next step. The above steps were repeated until there was no significant peak in the residual. The standard stop criterion of a signal-to-noise ratio $(S/N) > 4.0$ (Breger et al. 1993) was chosen to extract all significant frequencies. The uncertainties of all frequencies were calculated following the method provided by Montgomery & Odonoghue (1999). We note a higher detection threshold ($S/N = 5.4$) was

[3] TASOC database: https://tasoc.dk.

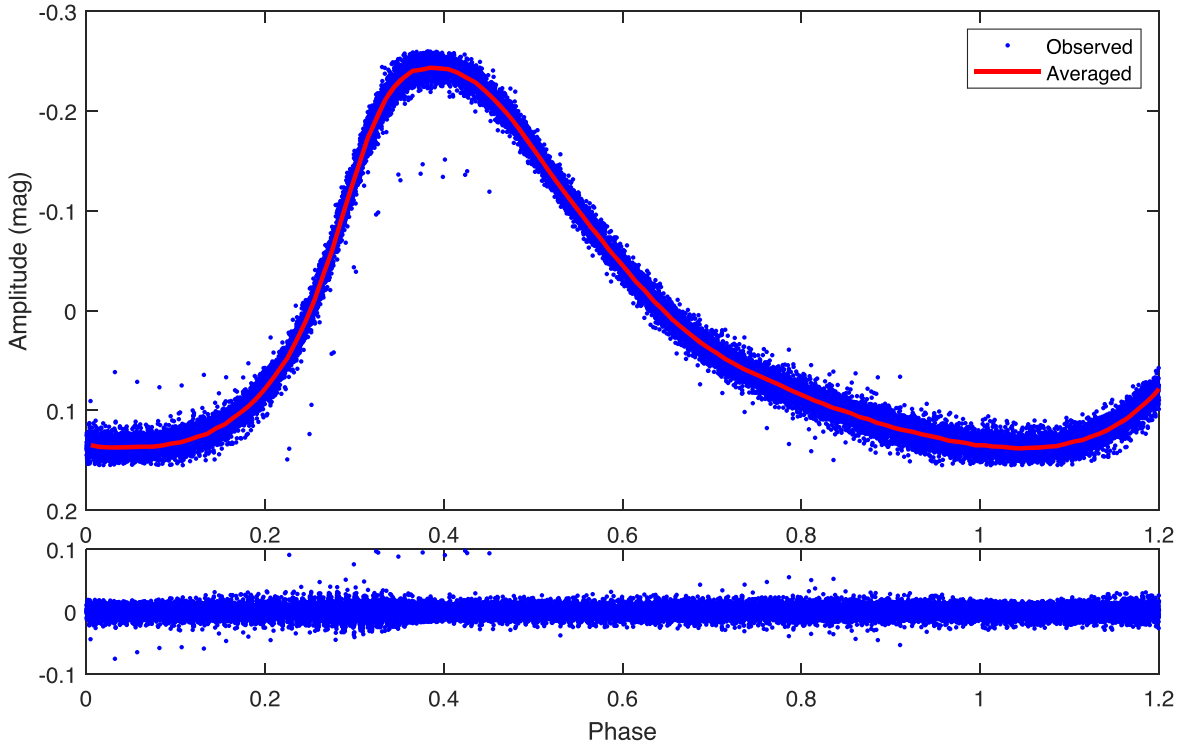

Figure 2. Phase diagram of GSC 4552-1498, folded by the frequency $F = 17.9176(7)\ \mathrm{day}^{-1}$. The obvious light variation of rapid climb and slow descent is typical for a HADS star.

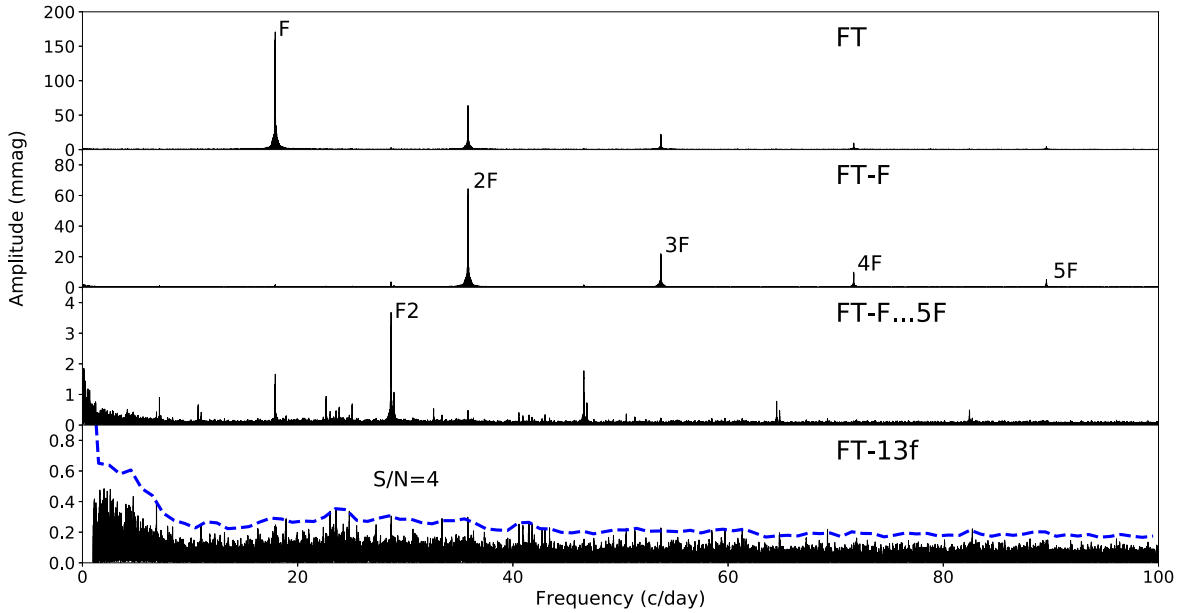

Figure 3. Fourier amplitude spectra of the frequency pre-whitening process for the light curves of GSC 4552-1498. Top panel, the initial Fourier amplitude spectra of the light curve, where the highest peak is $F = 17.9176(7)\ \mathrm{day}^{-1}$. The second panel, amplitude spectra of the residuals after subtracting the F, which shows four harmonic frequencies of F. The third panel shows amplitude spectra after subtracting the F and its harmonic frequencies, where the independent frequency $F2$ is marked. The bottom panel shows the residual after the fit shown in Table 2. Dotted curve refers to detection limit of $\mathrm{S/N} = 4.0$.

suggested to be a reliable and safe condition for time series data from space mission such as the Kepler K2 mission (Baran et al. 2015). Adopting this higher detection threshold does not influence the result of frequency analysis of this star.

The initial amplitude spectra was shown in the top panel of Figure 3, in which the frequency of the highest amplitude peak (F) was labeled. We removed F to produce the amplitude spectra in the second panel, where the four harmonic frequencies of F were visible. The last panel shows the amplitude spectra of the residuals after 13 detected frequencies were removed from the data. Following Breger et al. (1993), we drew the detection limit at an $\mathrm{S/N} = 4.0$ for the judgment of a significant peak. There is no obvious peak in the residuals and the overall distribution of the residual is typical noise.

Table 1
Basic Properties of GSC 4552-1498

Parameters	GSC 4552-1498	References
Brightness	12.655 mag	a
P	0.05581096 days	b
$T_{\rm eff}$	7615 K	a
log g	4.34248 dex	a
B	13.047 mag	a
V	12.987 mag	a
J	12.395 mag	a
H	12.264 mag	a
K	12.228 mag	a
R	12.77 mag	a
Gaia	12.8319 mag	a
M_v	2.312 ± 0.263 mag	b
$M_{\rm bol}$	2.344 ± 0.264 mag	b
L	$9.09 \pm 2.50\ L_{\odot}$	b
M	$1.68 \pm 0.10\ M_{\odot}$	b

Note. (a) These parameters are available in the TASOC; (b) Jafarzadeh & Poro (2017).

Table 2
Multifrequency Solution of the Light Curves of GSC 4552-1498 (denoted by f_{Si})

f_{Si}	Frequency ($\rm day^{-1}$)	Amplitude (mmag)	S/N	Identification
1	17.9176(7)	170.8	1042.4	F
2	35.8352(2)	64.4	721.3	2F
3	53.7529(1)	22.0	394.8	3F
4	71.6705(2)	10.0	177.8	4F
5	89.5882(1)	5.2	104.9	5F
6	28.6803(5)	3.7	34.5	F2
7	46.5980(7)	1.8	25.1	F+F2
8	22.6424(1)	0.9	10.9	F1
9	7.1546(1)	0.9	9.3	2F–F2
10	64.5156(2)	0.8	14.1	2F+F2
11	25.0722(2)	0.7	8.3	3F–F2
12	10.7628(4)	0.7	10.2	F2–F
13	82.4335(3)	0.5	9.2	3F+F2

Note. A total of 13 significant frequencies were detected, with S/N ratio larger than 4.0. Among these frequencies, there are three independent frequencies F, $F1$, and $F2$, four harmonic frequencies, and six combined frequencies.

The solutions of 13 frequencies with $\rm S/N > 4.0$ are listed in Table 2, including two frequencies that are consistent with those found by Jafarzadeh & Poro (2017) and 11 frequencies newly detected in this work. The frequency of the highest amplitude was usually assumed to be the fundamental radial mode, since the light variations were dominated by this frequency. Therefore, we marked f_{S1} as F in Table 2. The period ratio of $P_1/P_0 = f_{S1}/f_{S8} = 0.791$ is very close to the result (0.756–0.787) from Petersen & Christensen-Dalsgaard (1996). So f_{S8} may be the first overtone (1O) or a non-radial mode, which will be discussed in Section 5. And f_{S1} and f_{S6} have a period ratio of 0.625 (0.611–0.632) identifying f_{S6} as the second overtone radial mode (Breger 2000; Petersen & Christensen-Dalsgaard 1996; Stellingwerf 1979). Therefore, we marked f_{S8} and f_{S6} as $F1$ and $F2$, respectively. We note these two independent frequencies were first identified in this study. Due to this discovery, the source GSC 4552-1498 was no longer a single mode as previously thought. Another similar sample is KIC 10975348 (Yang et al. 2021), in which a low-amplitude frequency was detected recently, by using the Kepler data. It is very encouraging that in the space era, more sources with much weaker pulsation modes could be detected while it might be missed (i.e., falling in the noise) in the ground-based era. Since mode identification is of great importance in seismic modeling, and hence the study of stellar structure and evolution, we urge that a larger such sample is still needed in the near future.

4. $O-C$ Diagram

We used the $O-C$ technique to detect the long-term period changes of GSC 4552-1498. $O-C$ is the difference between the observed and calculated maximum times (Sterken 2005). The observed times of maximum light were determined by fitting the light curves. We made a second-order polynomial fit to a part of the light curves around each maximum. Generally, we chose a range with an amplitude of around one-third of the full amplitude, since this section of the light curves can reach a satisfactory fit. The fitting errors typically $0.00001\ \rm day^{-1}$ were estimated using Monte Carlo simulations (Lenz & Breger 2005). Finally, 1102 new maximum times were obtained from the TESS data and listed in Table A1 in the Appendix.

In order to make $O-C$ analysis of GSC 4552-1498, the newly determined times of maximum light were considered together with those provided by earlier studies: the maxima with numbers 19, 13, 20, 7, 16, and 4 obtained by Wils et al. (2009, 2012, 2013, 2014, 2015) and Jafarzadeh & Poro (2017), respectively. Then, these times of maximum light from ground-based observations (total 79, summarized in Table A2 in the Appendix), which were originally in HJD, were converted to BJD to be consistent in both timescale and format with the TESS data.

A total of 1181 maxima were collected. To obtain the calculated times of maximum light, $O-C$ values and their corresponding cycles, we fitted the 1181 maximum times with a straight-line and derived a new ephemeris formula:

$$\begin{aligned} \mathrm{BJD}_{\max} &= T_0 + P \times E \\ &= 2{,}453{,}321.534716(4) + 0.055811(0) \times E, \end{aligned} \quad (2)$$

where T_0, P, and E are the initial epoch, period, and the cycle number, respectively. And this ephemeris formula is consistent with the linear ephemeris given by Jafarzadeh & Poro (2017): $T = 2{,}453{,}321.53540 + 0.05581097 \times E$. All the $O-C$ values and the corresponding cycle numbers are listed in Tables A1 and A2 in the Appendix, respectively. The $O-C$ diagram is shown in Figure 4, where the blue dots represent the previous 79 points and the red dots are the 1102 new points.

We made a second-order polynomial fit to the 1181 points. The new ephemeris was obtained:

$$\begin{aligned} \mathrm{BJD}_{\max} &= 2{,}453{,}321.535993(2) + 0.055811(0) \times E \\ &\quad + 4.74(7) \times 10^{-13} \times E^2, \end{aligned} \quad (3)$$

with the standard deviation of the fitting residuals of 0.00026 day.

In the lower instability strip where the δ Scuti stars are found, stellar evolution theory predicts an increasing period in most of stars (Breger & Pamyatnykh 1998). And in pulsating stars, when a pulsation period changes linearly with time, the $O-C$ diagram will show a parabolic form that rises or falls depending on whether the period is increasing or decreasing (Sterken 2005). For GSC 4552-1498, from the $O-C$ diagram in Figure 4, the parabolic fit reveals a continuously increasing

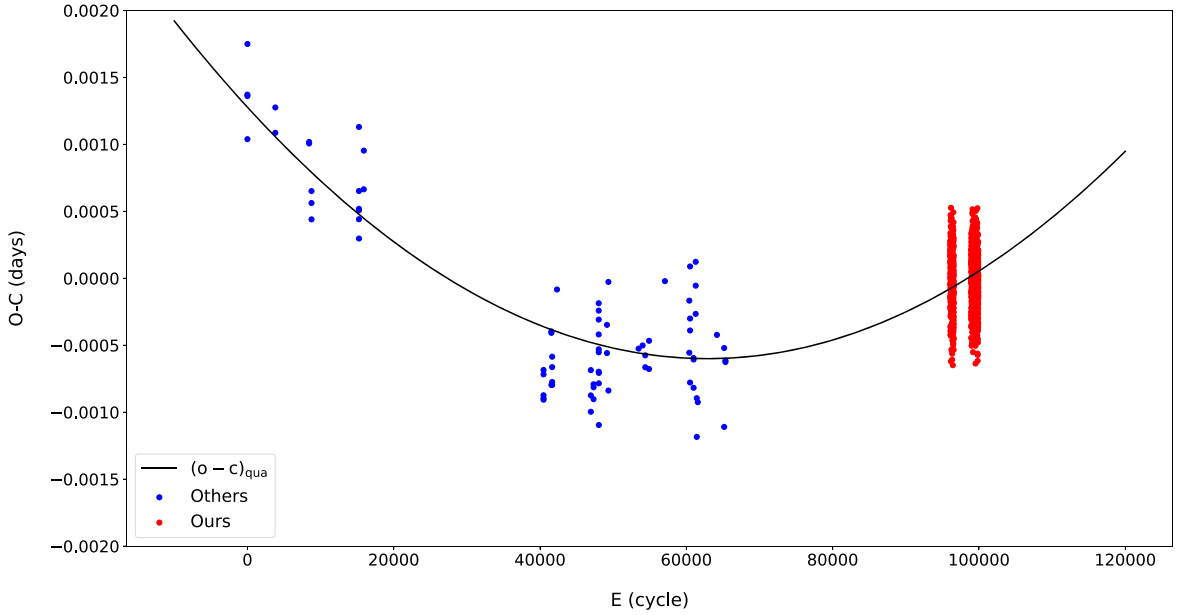

Figure 4. $O-C$ diagram of GSC 4552-1498, based on 1181 times of maximum light. The $O-C$ values are in days. Blue dots represent the previous 79 points and red dots are the 1102 new points. The black solid line shows the fit related to a continuously increasing period change.

period change. From Equation (3), the quadratic term indicates the rate of period change $(1/P)(dP/dt) = 1.11(3) \times 10^{-7}$ yr^{-1}.

5. Stellar Models and Fitting Results

We constructed a grid of evolutionary models of stars and calculated their corresponding adiabatic frequencies using the submodule "*pulse_adipls*" of the Modules for Experiments in Stellar Astrophysics (MESA v10398; Paxton et al. 2011, 2013, 2015, 2018, 2019). In the grid, the stellar mass ranges from 1.4–2.0 $M_{\odot}$ with a step of 0.02 $M_{\odot}$, and metallicities ranging from 0.002−0.030 with a step of 0.002. For the helium abundance Y, we adopted $Y = 0.249 + 1.33\,Z$ as a function of Z. Besides, the classical mixing length theory of Bohm–Vitense (1958) with $\alpha = 1.9$ (Paxton et al. 2013) was adopted. The effect of stellar rotation was not included in our calculations since the HADS star usually rotates slowly (McNamara 2000). Each model in the above grid was evolved from the zero-age MS to the post-MS stage, to give the pulsation frequencies of radial ($\ell = 0$) and/or non-radial with $\ell = 1$ and $\ell = 2$. Then by using the method from Chen et al. (2019), i.e., Equation (5), χ^2 method), the goodness of fit can be obtained, by comparing model frequencies with the observed frequencies F, $F1$, and $F2$.

In Figure 5, we present the changes of $1/\chi^2$ as a function of metallicity Z (top panel) and mass M (bottom panel), with $F1$ taken as radial 1O (blue circles) and non-radial (red circles) mode, respectively. Each circle represents one minimum value of χ^2 for each specific model. We note the blue circles are more concentrated along smaller value of $1/\chi^2$, hence larger χ^2, and then lower likelihood of the fitting, while the red circles spread widely, and may have much smaller χ^2. Therefore, we suggest $F1$ is more likely to be a non-radial mode. And It can be seen clearly that the metallicity Z converges from 0.008–0.018, and the mass M from 1.52–1.72 $M_{\odot}$, which is within the range of typical value of δ Scuti stars.

To select the best-fitting models, we chose a threshold of $\chi^2 = 0.02$ (horizontal line in the figures), which results in 10 candidate models, as listed in Table 3. These models can clearly be divided into two subgroups, that is to say, the metal-poor subgroup (with $Z = 0.008$), and the metal-rich subgroup (with Z around 0.016). Accordingly, the mass of this star was suggested to be $M = 1.52^{+0.02}_{-0.00}$ in the case of $Z = 0.008$, and $M = 1.56^{+0.16}_{-0.02}$ if Z around 0.016, if taking models with the smallest χ^2 as the best-fitting models. Interestingly, models with mass $M = 1.54\,M_{\odot}$ can have two different metallicities, i.e., 0.008 and 0.018, which is due to different mode identifications of $F1$, with $\ell = 1$ and 2, respectively, as marked in Table 3. We note, in any case, the frequency $F1$ should be identified as a non-radial mode.

And we stress that, from Table 3 and Figure 5, the mass–metallicity degeneracy of the fittings is notable, and similar to that found by Bowman et al. (2021). Due to the large uncertainties of Z and the mass–metallicity degeneracy, we suggest high-resolution spectra is highly desired in the future, which would help not only give an accurate determination of the metallicity that may break the degeneracy, but also provide other parameters, such as effective temperature and rotational rate, which could further narrow down the parameter space of this star.

In addition, we calculated the rate of period change in either case (models in Table 3) in order to compare with observations. The results were listed in Table 3 (the second to the last column), as well. It is notable that all predicted rates of period change are significantly smaller than the value we obtained from $O-C$, by about two orders of magnitude. We note this discrepancy has long been established for δ Scuti stars (Rodríguez et al. 1995; Breger & Pamyatnykh 1998; Rodríguez & Breger 2001; Bowman et al. 2016, 2021), which may not be accounted for solely by stellar evolution. The possible reason is still uncertain, possibly due to nonlinear mode interaction, resonant mode coupling (Breger & Montgomery 2014) and/or in special cases mass accretion in binaries (DY Pegasi; Xue & Niu 2020), all of which still need further investigation. A larger sample of δ Scuti stars with similar temporal properties to GSC 4552-1498 is no doubt helpful to further address this issue.

In Figure 6, we showed the evolutionary tracks from the zero-age MS to the post-MS stage for models in Table 3 in

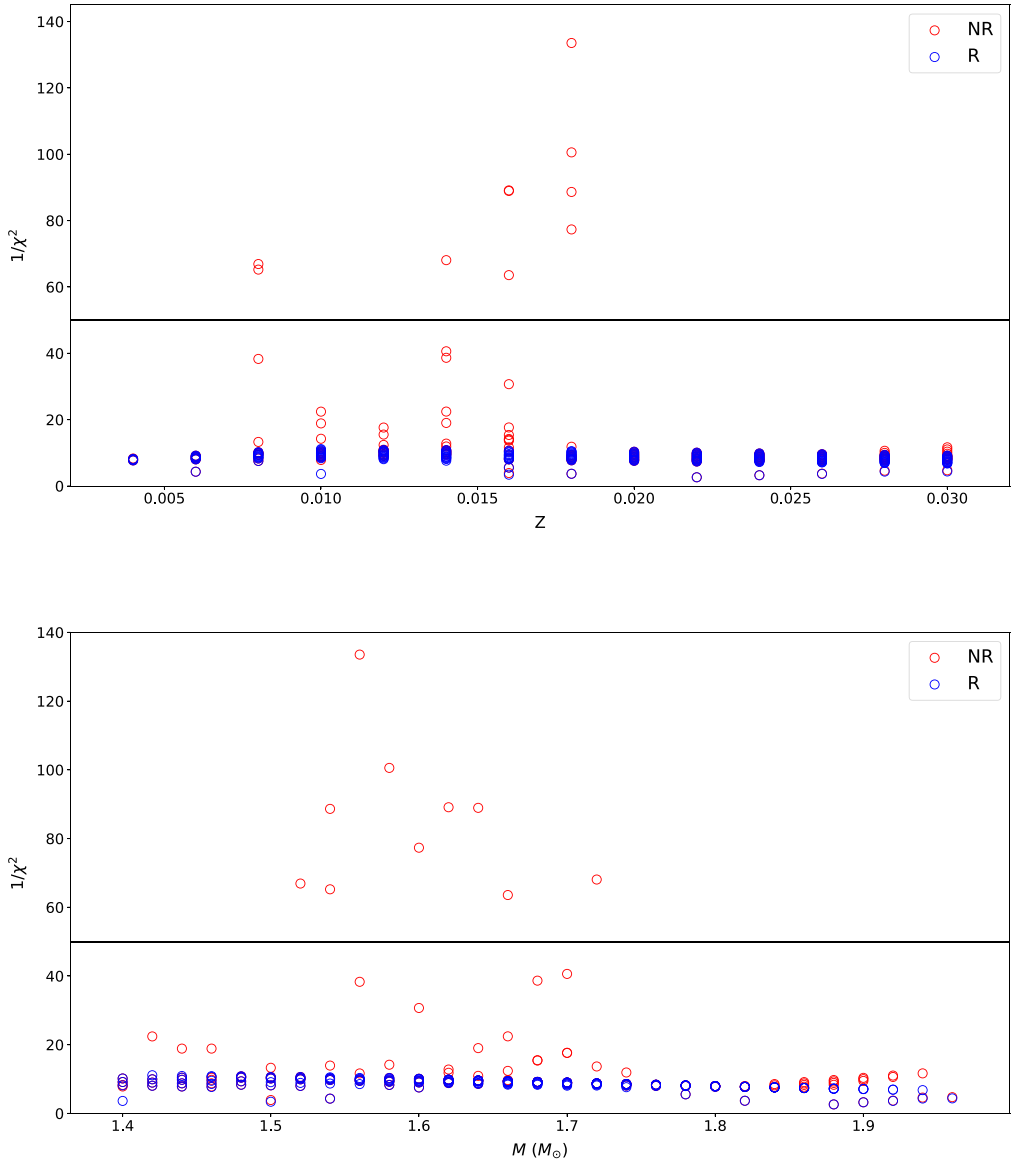

Figure 5. Visualization of the resulting $1/\chi^2$ as a function of metallicity Z (top panel) and stellar mass M (bottom panel), respectively. The red circles mark $F1$ taken as radial (R) 1O and blues circles non-radial (NR) mode, respectively. Ten candidate models were selected with a threshold of $\chi^2 \leqslant 0.02$ (horizontal black line), as listed in Table 3.

Table 3
Candidate Models with $\chi^2 \leqslant 0.02$

Mass ($M_\odot$)	Z (dex)	$T_{\rm eff}$ (K)	$L/L_\odot$	F (c days^{-1})	$F1$ (ℓ, n) (c days^{-1})	$F2$ (c days^{-1})	$(1/P)(dP/dt)$ (yr^{-1})	χ^2
1.52	0.008	7700.60	8.60	17.8196	22.3405 (1, 1)	28.1392	5.49×10^{-10}	0.0145
1.54	0.008	7779.01	9.03	18.1020	22.6703 (1, 1)	28.5744	5.63×10^{-10}	0.0149
1.54	0.018	7013.48	5.90	18.0473	22.7719 (2, 0)	28.6620	2.92×10^{-10}	0.0109
1.56	0.018	7083.43	6.21	18.0079	22.5679 (2, 0)	28.5868	3.07×10^{-10}	0.0073
1.58	0.018	7160.02	6.53	18.0511	22.5404 (2, 0)	28.6401	3.21×10^{-10}	0.0096
1.60	0.018	7230.77	6.87	18.0058	22.5137 (2, 0)	28.5603	3.36×10^{-10}	0.0125
1.62	0.016	7438.58	7.76	18.0554	22.7286 (2, 0)	28.5950	3.92×10^{-10}	0.0108
1.64	0.016	7517.68	8.15	18.0725	22.7151 (2, 0)	28.6133	4.06×10^{-10}	0.0109
1.66	0.016	7582.41	8.55	18.0044	22.7248 (2, 0)	28.4990	4.03×10^{-10}	0.0153
1.72	0.014	7948.37	10.52	18.0894	22.6375 (2, 0)	28.5598	5.20×10^{-10}	0.0142

Note. (ℓ, n) are the spherical harmonic degree and the radial order of the model frequency, respectively. The (ℓ, n) of F of all candidate models is (0, 0), while $F2$ is (0, 2).

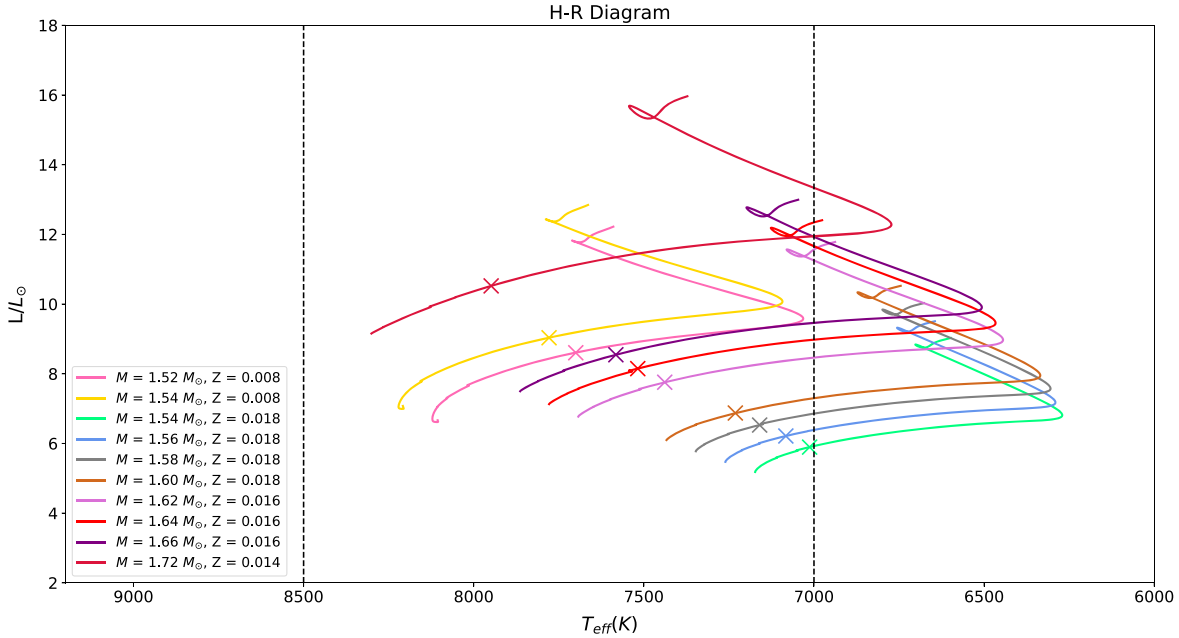

Figure 6. Evolutionary tracks from the zero-age MS to the post-MS for the 10 candidate models, as listed in Table 3. The crosses mark the minimum χ^2 for each specific model by fitting the calculated F, $F1$, and $F2$ with the observed values. The two vertical dotted lines mark $T_{\rm eff}$ at 7000 and 8500 K, respectively.

order to better understand the evolution of GSC 4552-1498. The color lines represent different combinations of metallicity Z and mass M. The crosses mark the minimum χ^2 for each specific model. In order to be in line with the derived value of $T_{\rm eff}$ given by (Jafarzadeh & Poro 2017, i.e., 7766 ± 59 K) and TESS website (7615 K), models with a broader range of temperature between 7000 and 8500 K were adopted. We note all these models suggest that GSC 4552-1498 is located on the MS in the H-R diagram. When compared with another five HADS stars (see Table 12 in Xue et al. 2018), we note GSC 4552-1498 has the shortest P_0. Using the basic pulsation relation $P\sqrt{\bar{\rho}/\rho_\odot} = {\rm Q}$ (P is the period and Q is the pulsation constant), the mean density $\bar{\rho}$ could be roughly estimated. Then this leads to the largest $\bar{\rho}$ for GSC 4552-1498 among the six HADS, revealing that GSC 4552-1498 is still at an earlier stage than the others. Our result is consistent with the tendency derived by Xue et al. (2018), that the lower the fundamental frequency is, the later the star would have evolved into (also see Figure 9 in Xue et al. 2018).

6. Summary

By analyzing the light variations of GSC 4552-1498 using photometric data delivered by the TESS mission, we detected 13 significant frequencies (see Table 2) including three independent frequencies $F = 17.9176\,{\rm day}^{-1}$, $F1 = 22.6424\,{\rm day}^{-1}$ and $F2 = 28.6803\,{\rm day}^{-1}$. Among them, $F1$ and $F2$ were newly detected in this work and F is also consistent with previous study (see Table 1, Jafarzadeh & Poro 2017). And according to the period ratio of $F/F2$, the independent frequency $F2$ is the second radial mode.

We obtained the $O-C$ diagram with 1181 times of maximum light including 1102 from the TESS mission in this work (see Table A1) and 79 from the literature (see Table A2), and derived a new ephemeris: ${\rm BJD}_{\rm max} = T_0 + P \times E = 2453321.534716(4) + 0.055811(0) \times E$. In addition, the change of period of GSC 4552-1498 was determined for the first time in this work, i.e., increasing continuously with a rate of $(1/P)(dP/dt) = 1.11(3) \times 10^{-7}$ yr^{-1}, which is about two orders of magnitude larger than predicted by evolution theories (see Table 3, the second to the last column). The possible reason might be related to nonlinear mode interaction but still need further investigation.

The stellar evolutionary models were constructed with different mass M and metallicity Z using MESA. By comparing the observed values of F, $F1$, and $F2$ with models, we suggest that $F1$ is a non-radial mode (see Table 3). Due to the mass–metallicity degeneracy, the mass of this star can still not be determined conclusively, that is to say, $M = 1.52^{+0.02}_{-0.00}$ if $Z = 0.008$, and $M = 1.56^{+0.16}_{-0.02}\ M_\odot$ if Z is around 0.016. We suggest high-resolution spectral observation in the future is needed to accurately determine the stellar parameters. Consequently, GSC 4552-1498 is no longer a single-mode HADS star, having a continuously increasing period change, and located on the MS stage in the H-R diagram.

We would like to thank the TESS science team for providing such excellent data. This research is supported by the program of the National Natural Science Foundation of China (grant Nos. 11573021, U1938104, and 12003020).

Appendix

In Tables A1 and A2, we listed all the O − C values and the corresponding cycle numbers, respectively.

Table A1
1102 New Times of Maximum Light and $O-C$ Values of GSC 4552-1498

BJD (2450000+)	E	$O-C$ (day)	BJD (2450000+)	E	$O-C$ (day)	BJD (2450000+)	E	$O-C$ (day)
8683.4103	96,072	0.000278	8709.4737	96,539	−0.000044	8868.1997	99,383	−0.000435
8683.4657	96,073	−0.000133	8709.5298	96,540	0.000245	8868.4235	99,387	0.000121
8683.5219	96,074	0.000256	8709.5850	96,541	−0.000366	8868.5912	99,390	0.000388
8683.6892	96,077	0.000123	8709.6410	96,542	−0.000177	8868.6466	99,391	−0.000023
8683.8009	96,079	0.000201	8709.6968	96,543	−0.000188	8868.7028	99,392	0.000366
8683.8563	96,080	−0.000210	8709.7527	96,544	−0.000099	8868.7581	99,393	−0.000145
8683.9124	96,081	0.000079	8709.8085	96,545	−0.000110	8870.9907	99,433	0.000016
8683.9683	96,082	0.000168	8709.9204	96,547	0.000168	8871.0467	99,434	0.000205
8684.0239	96,083	−0.000043	8709.9757	96,548	−0.000343	8871.3257	99,439	0.000151
8684.0800	96,084	0.000246	8710.0316	96,549	−0.000254	8871.3813	99,440	−0.000060

Note. $T_{\max}$ is the observed times of maximum light of GSC 4552-1498. E: Cycle number. $O-C$ is in days. E and $O-C$ are based on the ephemris formula: $\mathrm{BJD}_{\max} = T_0 + P \times E = 2453321.534716(4) + 0.055811(0) \times E$. Table A1 is published in its entirety in the machine-readable format. A portion is shown here for guidance regarding its form and content.

(This table is available in its entirety in machine-readable form.)

Table A2
79 Previous Times of Maximum Light and $O-C$ Values of GSC 4552-1498

BJD (2450000+)	E	$O-C$ (day)	S	BJD (2450000+)	E	$O-C$ (day)	S
3321.5361	0	0.001372	1	6001.4116	48,017	−0.000308	3
3321.5919	1	0.001361	1	6001.4673	48,018	−0.000419	3
3321.6481	2	0.001750	1	6001.5230	48,019	−0.000530	3
3321.7032	3	0.001039	1	6001.5791	48,020	−0.000241	3
3534.3990	3814	0.001087	1	6001.6346	48,021	−0.000552	3
3534.4550	3815	0.001276	1	6002.3041	48,033	−0.000784	3
3792.3016	8435	0.001018	1	6002.3596	48,034	−0.001095	3
3792.3574	8436	0.001007	1	6002.4158	48,035	−0.000706	3
3810.3281	8758	0.000562	1	6064.4780	49,147	−0.000347	3
3810.3840	8759	0.000651	1	6064.5336	49,148	−0.000558	3
3810.4396	8760	0.000440	1	6075.5289	49,345	−0.000027	3
4172.3742	15,245	0.000652	1	6075.5839	49,346	−0.000838	3
4172.4298	15,246	0.000441	1	6305.6930	53,469	−0.000525	4
4172.4863	15,247	0.001130	1	6336.5007	54,021	−0.000501	4
4172.5415	15,248	0.000519	1	6356.5925	54,381	−0.000664	4
4172.5973	15,249	0.000508	1	6356.6484	54,382	−0.000575	4
4172.6529	15,250	0.000297	1	6385.5028	54,899	−0.000467	4
4209.3211	15,907	0.000665	1	6385.5584	54,900	−0.000678	4
4209.3772	15,908	0.000954	1	6506.4457	57,066	−0.000021	4
5580.4286	40,474	−0.000873	2	6692.6865	60,403	−0.000556	5
5580.4846	40,475	−0.000684	2	6692.7427	60,404	−0.000167	5
5580.5402	40,476	−0.000895	2	6698.3790	60,505	−0.000778	6
5580.5960	40,477	−0.000906	2	6698.4352	60,506	−0.000389	6
5580.6520	40,478	−0.000718	2	6698.4911	60,507	−0.000300	6
5640.3697	41,548	−0.000796	2	6698.5473	60,508	0.000089	6
5640.3701	41,548	−0.000396	2	6725.3359	60,988	−0.000595	5
5640.4259	41,549	−0.000407	2	6725.3917	60,989	−0.000606	5
5646.2858	41,654	−0.000663	2	6725.4473	60,990	−0.000817	5
5646.3415	41,655	−0.000774	2	6741.3542	61,275	−0.000055	5
5646.3975	41,656	−0.000585	2	6741.4098	61,276	−0.000266	5
5646.4531	41,657	−0.000796	2	6741.4660	61,277	0.000123	5
5683.4007	42,319	−0.000084	2	6749.6131	61,423	−0.001184	5
5941.4142	46,942	−0.000874	3	6749.6692	61,424	−0.000895	5
5941.4702	46,943	−0.000685	3	6757.4269	61,563	−0.000925	5
5941.5257	46,944	−0.000996	3	6903.4290	64,179	−0.000423	5
5962.2876	47,316	−0.000791	3	6958.6254	65,168	−0.001110	5
5962.3433	47,317	−0.000902	3	6958.6818	65,169	−0.000521	5
5962.3992	47,318	−0.000813	3	6968.2812	65,341	−0.000614	5
6001.3001	48,015	−0.000186	3	6968.3370	65,342	−0.000625	5
6001.3554	48,016	−0.000697	3				

Note. $T_{\max}$ is the observed times of maximum light in BJD 2450000. E: Cycle number. $O-C$ is in days. E and $O-C$ are based on the ephemris formula: $\mathrm{BJD}_{\max} = T_0 + P \times E = 2453321.534716(4) + 0.055811(0) \times E$. Source [S]: (1) Wils et al. (2009); (2) Wils et al. (2012); (3) Wils et al. (2013); (4) Wils et al. (2014); (5) Wils et al. (2015); (6) Jafarzadeh & Poro (2017).

(This table is available in machine-readable form.)

ORCID iDs

Zhao-Yu Zuo https://orcid.org/0000-0001-6693-586X
Tao-Zhi Yang https://orcid.org/0000-0002-1859-4949
Xing-Hao Chen https://orcid.org/0000-0003-3112-1967

References

Aerts, C. 2021, RvMP, 93, 015001
Aerts, C., Christensen-Dalsgaard, J., & Kurtz, D. W. 2010, Asteroseismology, Astronomy and Astrophysics Library (Berlin: Springer), 2010
Antoci, V., Cunha, M., Houdek, G., et al. 2014, ApJ, 796, 118
Antoci, V., Cunha, M. S., Bowman, D. M., et al. 2019, MNRAS, 490, 4040
Balona, L. A., & Dziembowski, W. A. 2011, MNRAS, 417, 591
Balona, L. A., Lenz, P., Antoci, V., et al. 2012, MNRAS, 419, 3028
Baran, A. S., Koen, C., & Pokrzywka, B. 2015, MNRAS, 448, L16
Böhm-Vitense, E. 1958, ZAp, 46, 108
Borucki, W. J., Koch, D., Basri, G., et al. 2010, Sci, 327, 977
Bowman, D. M. 2017, Amplitude Modulation of Pulsation Modes in Delta Scuti Stars (Berlin: Springer), 2017
Bowman, D. M., Hermans, J., Daszyńska-Daszkiewicz, J., et al. 2021, MNRAS, 504, 4039
Bowman, D. M., & Kurtz, D. W. 2018, MNRAS, 476, 3169
Bowman, D. M., Kurtz, D. W., Breger, M., et al. 2016, MNRAS, 460, 1970
Breger, M. 2000, in ASP Conf. Ser. 210, Delta Scuti and Related Stars, ed. M. Breger & M. Montgomery (San Francisco, CA: ASP), 3
Breger, M., & Montgomery, M. H. 2014, ApJ, 783, 89
Breger, M., & Pamyatnykh, A. A. 1998, A&A, 332, 958
Breger, M., Stich, J., Garrido, R., et al. 1993, A&A, 271, 482
Chen, X., Li, Y., & Zhang, X. 2019, ApJ, 887, 253
Holdsworth, D. L., Smalley, B., Gillon, M., et al. 2014, MNRAS, 439, 2078
Jafarzadeh, S. J., & Poro, A. 2017, NewA, 54, 86
Lenz, P., & Breger, M. 2005, CoAst, 146, 53
McNamara, D. H. 2000, in ASP Conf. Ser. 210, Delta Scuti and Related Stars, ed. M. Breger & M. Montgomery (San Francisco, CA: ASP), 373
Montgomery, M. H., & Odonoghue, D. 1999, DSSN, 13, 28
Murphy, S. J., Saio, H., Takada-Hidai, M., et al. 2020, MNRAS, 498, 4272
Murphy, S. J., Shibahashi, H., & Kurtz, D. W. 2013, MNRAS, 430, 2986
Paxton, B., Bildsten, L., Dotter, A., et al. 2011, ApJS, 192, 3
Paxton, B., Cantiello, M., Arras, P., et al. 2013, ApJS, 208, 4
Paxton, B., Marchant, P., Schwab, J., et al. 2015, ApJS, 220, 15
Paxton, B., Schwab, J., Bauer, E. B., et al. 2018, ApJS, 234, 34
Paxton, B., Smolec, R., Schwab, J., et al. 2019, ApJS, 243, 10
Petersen, J. O., & Christensen-Dalsgaard, J. 1996, A&A, 312, 463
Qian, S.-B., Li, L.-J., He, J.-J., et al. 2018, MNRAS, 475, 478
Ricker, G. R., Winn, J. N., Vanderspek, R., et al. 2014, Proc. SPIE, 9143, 914320
Ricker, G. R., Winn, J. N., Vanderspek, R., et al. 2015, JATIS, 1, 014003
Rodríguez, E., & Breger, M. 2001, A&A, 366, 178
Rodríguez, E., López de Coca, P., Costa, V., & Martín, S. 1995, A&A, 299, 108
Stellingwerf, R. F. 1979, ApJ, 227, 935
Sterken, C. 2005, in ASP Conf. Ser. 335, The Light-Time Effect in Astrophysics, ed. C. Sterken (San Francisco, CA: ASP), 3
Uytterhoeven, K., Moya, A., Grigahcène, A., et al. 2011, A&A, 534, A125
Wils, P., Ayiomamitis, A., Robertson, C. W., et al. 2014, IBVS, 6122, 1
Wils, P., Ayiomamitis, A., Vanleenhove, M., et al. 2013, IBVS, 6049, 1
Wils, P., Hambsch, F.-J., Vanleenhove, M., et al. 2015, IBVS, 6150, 1
Wils, P., Kleidis, S., Hambsch, F.-J., et al. 2009, IBVS, 5878, 1
Wils, P., Panagiotopoulos, K., van Wassenhove, J., et al. 2012, IBVS, 6015, 1
Xue, H.-F., Fu, J.-N., Fox-Machado, L., et al. 2018, ApJ, 861, 96
Xue, H.-F., & Niu, J.-S. 2020, ApJ, 904, 5
Yang, T.-Z., & Esamdin, A. 2019, ApJ, 879, 59
Yang, T.-Z., Esamdin, A., Fu, J.-N., et al. 2018a, RAA, 18, 002
Yang, T.-Z., Esamdin, A., Song, F., et al. 2018b, ApJ, 863, 195
Yang, T.-Z., Sun, X.-Y., Zuo, Z.-Y., et al. 2021, AJ, 161, 27